Soft Matter

PAPER

Normal and shear interactions between high grafting density polymer brushes grown by atom transfer radical polymerization

Wei-Po Liao, Ian G. Elliott, Roland Faller and Tonya L. Kuhl*

The normal and shear interactions in toluene of polystyrene polymer brushes with ultra-high surface coverage ranging from 15 to 70 mg m^{-2} formed by atom transfer radical polymerization were measured with a surface force apparatus. Significant hysteresis was observed between compression and separation cycles over the experiment time scale for all surface coverages. The magnitude of the hysteresis increased with increasing film thickness. The experimental relaxation time of the thickest brush layer was at least four orders of magnitude longer than that predicted by the Rouse model. Remarkably, the shear performance of the thickest brushes still demonstrated very good lubricity under compressions down to 35% solvent content. These findings are consistent with a reduction in solvent quality with compression leading to a shrinkage or collapse of the brush under high compression, while still maintaining a region of well solvated chains in the overlap region between the brushes. The results suggest the hysteresis in compression is primarily due to intra-brush entanglements and collapse of the brush layer rather than inter-brush entanglements and brush–brush interpenetration.

Introduction

Polymer brushes are frequently used to modify interfacial properties where they can act as steric stabilizers, adhesion modifiers, or enhance lubricity.[1–3] A polymer brush is formed when one end of the chain is confined to the interface or surface and the spacing between these anchor points is smaller than the polymer chain's radius of gyration, R_g. As the spacing between neighboring chains decreases, the chains are forced to stretch away normal to the grafting surface to decrease crowding. These structural changes due to osmotic crowding result in very different behaviors from free polymer chains in solution.[4,5] In typical experiments, the polymer brush layer is formed by a "grafting to" approach in which chains are selectively anchored to the surface through physical adsorption methods that rely on diblock polymer chains and preferential solvation or by functionalizing the chain end leading to strong electrostatic binding or chemical bond formation to the surface. In both cases, the grafting density of the brush is limited by steric hindrance between the surface grafted chains.[6]

Because the brush structure and its physical properties depend intimately on the chain molecular weight, surface coverage, and solvent quality,[7–9] polymer brushes can be used to tailor interfacial properties.[1–3] Motivated by the wide application potential of polymer brush systems, a large number of

theoretical,[5,10–14] experimental[15–19] and simulation[20–25] studies have been carried out in order to characterize and ultimately predict the properties of polymer brushes. In particular, the tribological behavior of polymer-bearing surfaces has drawn significant attention as ultra-low friction coatings.[26–31] For example, Klein *et al.*[26] found that the friction coefficient between mica surfaces grafted with end-functionalized polystyrene (PS) brushes in good solvent conditions was two orders of magnitude lower than that of bare mica in toluene. Similarly, Raviv *et al.*[28] found similar low friction behavior with physically adsorbed poly(ethylene oxide) (PEO) bearing surfaces in good solvent condition under moderate compressions. For high shear rates and high compression, some loss of the polymer brush layer was observed and a transition of the shear interface from polymer/polymer to polymer/substrate was suggested. A detailed comparison of normal and shear behavior in good and theta solvent conditions was carried out by Schorr *et al.*[31] using amphiphilic polystyrene–poly(vinylpyridine) (PS–P2VP) diblocks. The best lubricant performance was found for good solvent conditions and shear-thinning behavior was observed with increasing sliding velocity. Using the same system, Forster *et al.*[32] found similar behavior where the onset of detectable shear force was found to shift to higher compression ratios as the solvent quality increased. Thus, the compression and interpenetration of opposing brush layers plays an important role in their frictional properties and the extent of interpenetration has been shown to increase with compression ratio and grafting density.[29,33,34] At a molecular level, recent molecular dynamic simulations have

Department of Chemical Engineering and Materials Science, University of California, Davis, CA 95616, USA. E-mail: tlkuhl@ucdavis.edu

directly linked better lubrication behavior in good solvent conditions to fewer inter-brush contacts.[35] However, these previous studies were on dilute to semi-dilute brushes and the properties of ultra-high grafting density brushes have not yet been systematically studied.

Intrinsically, steric overlap between neighboring chains limits "grafting-to" polymer brushes to the dilute or semi-dilute grafting density regime. This can constrain the practical application needs of a stable and durable surface, particularly under high load. In contrast, the "grafting from" method where the polymer chain grows monomer by monomer from a surface using living polymerizations[36] can yield much higher grafting densities. However, only a handful of experiments have studied brush properties in this regime. Ruths et al.[37] performed the first comprehensive measurements of the interaction force between "grafting-from" brushes by replacing the chemically inert mica surfaces typically used in the surface force apparatus (SFA) with thin silica films that could be functionalized with a covalently grafted ATRP initiator layer. High molecular weight polystyrene brushes were grown directly on the surfaces, however the high polydispersity of the chains made quantitative comparison to polymer theory challenging.[38] Subsequently, Yamamoto et al.[39,40] investigated poly(methyl methacrylate) (PMMA) brushes by AFM. Discrepancies between the experimentally measured force–distance profile and scaling predictions[41] were attributed to the fact that the polymer concentration under this highly grafted condition significantly exceeded the semi-dilute concentration range assumptions used in the scaling theory. The tribology properties of "grafted from" brushes have primarily been investigated macroscopically[42–44] using conventional ball-on-disk type tribometers. Sakata et al.[43] measured PMMA brushes in different solvent conditions including the dry state. As in the microscopic SFA measurements, the lowest dynamic friction coefficient was found in good solvent conditions. In contrast, Kobayashi et al.[42] found that the high density brushes of biocompatible polymer 2-methacryloyloxyethyl phosphorylcholine (MPC) had the best lubricant performance when in a high-humidity environment rather than when fully solvated in bulk water. They hypothesized that the dense brushes interpenetrated more in bulk water leading to higher friction compared to brushes in high humidity. Recently, Dunlop et al.[45] demonstrated a means to functionalize mica surfaces with a strongly adsorbed poly-initiator film in order to obtain high grafting densities of a surface-grown polyelectrolyte brush of poly[2-(methacryoyloxy)ethyl][29,46]trimethylammonium chloride (poly(METAC)). A small hysteresis was observed between the polyelectrolyte brushes during compression–decompression cycles which was attributed to attractive bridging interactions. Frictional properties were similar to earlier studies on polyelectrolyte brushes. This approach opens a straightforward means to carryout high resolution SFA experiments on high grafting density polymer layers.

In this work, an SFA was used to measure the normal and shear forces of high density "grafted from" polystyrene chains in toluene, a good solvent for polystyrene. The brushes were grown from silica films electron-beam deposited on mica enabling higher film thicknesses and grafting densities to be studied, while still preserving the high force and distance resolution of the SFA technique. In contrast to previous work on "grafted to" brushes at lower grafting densities that have primarily shown reversible compression forces, significant hysteresis was observed in the high density, "grafted from" system. The hysteresis, however, did not correlate with an increased friction between the brushes during shear force measurements at modest solvation. The work demonstrates that ultra-high density polymer brushes provide a very robust, low friction coating even under conditions where solvent quality maybe significantly reduced.

Experimental section

Surface functionalization of mica

To provide an appropriate substrate for ATRP synthesis of the grafted from polymer brush chains, a thin-coating of silica was electron beam (E-beam, AUTO-TECH II, CHA industries) deposited on freshly cleaved sheets of mica. The procedure used followed the methodology described by Vigil et al.[47] In the present work, the silica layer was 1000 Å silica layer. The thickness and the refractive index of the silica layer were further confirmed by ellipsometry (EL2, Rudolph) yielding values of thickness and the refractive index of 1048 ± 12 Å and 1.48 ± 0.01, respectively.[48] The root mean square roughness of the deposited silica was 6 Å over a 5 × 5 μm² area as determined by AFM and is consistent with the values previously reported by Vigil et al.[47] and Orozco-Alcaraz et al.[48]

The thickness and refractive index of the silica film was also characterized in the SFA using multiple beam interferometry prior to ATRP polymer film growth. Freshly cleaved mica with the desired thickness (3–4 μm) was first cut into one or two larger pieces (few cm²) and one smaller piece (few mm²). The smaller piece was not coated with silica and used as a reference system to determine the mica substrate thickness. Silica was then deposited on the larger mica piece(s). After silica deposition, the mica pieces were flipped and placed on another mica backing sheet. A ~550 Å silver layer was deposited on the mica side of both the small mica pieces and the silica deposited mica pieces. The coated mica surfaces were then glued, silver side down, onto cylindrically curved glass disks using an optical adhesive (NOA 61, Norland Product Inc.) and cured by exposure to UV light for 5 minutes. Details of the thickness and refractive index determination by multiple beam interferometry are provided later under the heading Thickness determination.

Atom transfer radical polymerization

Materials. Styrene was purchased from Fisher Scientific, Karstedt catalyst was purchased from Gelest, and all other chemicals were from Sigma-Aldrich. Styrene was stirred with CaH_2 overnight to remove any water and vacuum distilled to remove the inhibitor. The distilled styrene was stored at 4 °C under nitrogen. CuBr was stirred over glacial acetic acid overnight, filtered, and washed with large quantities of ethanol.

10-Undecenyl 2-bromoisobutyrate synthesis

10-Undecenyl 2-bromoisobutyrate, a precursor required for the initiator synthesis, was synthesized following the work of

Matyjaszewski *et al.*[49] A stir bar, 5.9 mL 10-undecen-1-ol, 5.3 mL triethylamine, and 50 mL dichloromethane were added to a 100 mL round bottom flask in an ice bath. 3.7 mL 2-bromoisobutyryl bromide were added to the flask dropwise over a period of 5 minutes. The flask was removed from the ice bath and stirred at room temperature for 15 hours. The solution was washed with 65 mL of 0.5 molar HCL, and then washed with 65 mL DI water 3 times. Solvent was removed by rotovap. The solution was run through a column of silica gel with 100 mL of a 25 : 1 hexane : ethyl acetate solvent solution. The solution was again rotovaped to remove hexane. This procedure yielded approximately 7.5 g of a clear liquid.

Initiator synthesis

The surface active initiator (11-(2-bromo-2-methyl)propionyloxy)undecyl trichlorosilane was synthesized following previous work.[50] 4.6 mL of 10-undecenyl 2-bromoisobutyrate and a stir bar were added to a 50 mL schlenk flask. The flask was sealed and purged with nitrogen. Three freeze–pump–thaw cycles followed to ensure no oxygen was in the flask or liquid. 82 μL of Karstedt catalyst (2.1–2.4% Pt in xylene) were added and the flask was transferred to an ice bath. 4.75 mL trichlorosilane was added dropwise to the solution. The flask was allowed to slowly warm to room temperature and stirred for five hours under nitrogen. The product was transferred to a round bottom flask and vacuum distilled at 30 mtorr. The distillation yielded 2.72 grams of initiator.

Initiator deposition

The silica surfaces glued on the SFA discs were cleaned prior to initiator deposition by stirring in acetone for 10 minutes, followed by rinsing with isopropyl alcohol, Millipore filtered water, pure ethanol, and then dried with nitrogen. The surfaces were then exposed to UV/ozone for 20 minutes to hydroxylate the surfaces. Afterwards, the substrates were placed in a gently stirred solution of 34 μL (11-(2-bromo-2-methyl)propionyloxy)undecyl trichlorosilane in 50 mL toluene for one hour. Upon removal of the substrates, partial dewetting of the toluene solution at the edge of the surfaces was evident of the formation of a self-assembled layer of initiator. The surfaces were then immediately rinsed in clean toluene (10 minute immersion with gentle stirring), removed and dried with nitrogen. Finally, the dry initiator coated surfaces were annealed at 75 °C to promote cross-polymerization and robust attachment of the initiator layer.

Polymerization

End-grafted polystyrene chains were synthesized from the initiator coated surfaces using established procedures.[50,51] A custom reaction flask was used which could be taken apart to add or remove the surfaces.[50] After placing the surfaces in the reaction flask, 124 mg CuBr, 10 mg CuBr$_2$, and a stir bar were added. The flask was sealed and evacuated and backfilled with nitrogen three times. In a separate Schlenk flask 10 mL styrene, 5 mL toluene, and 189 μL N,N,N',N',N''-pentamethyldiethylenetriamine (PMDETA) were added and oxygen was removed by performing three freeze–pump–thaw cycles. Afterwards, 13 μL

ethyl 2-bromoisobutyrate were added to the flask, and the solution was immediately transferred to the custom reaction flask at 90 °C using a syringe. The reaction was allowed to proceed for a designated time, generally three to eight hours. To quench the reaction at the designated time, the heat was turned off, the solution was exposed to air, and THF was added. Finally, the surfaces were stirred in hot toluene for 20 minutes to remove unreacted monomer and stirred in IPA for 20 minutes to remove copper salts.

Surface force apparatus

The surface force apparatus (SFA) technique has been widely used for measuring the interactions between two opposing surfaces as a function of separation and details of the instrument and measurements have been explicitly described elsewhere.[52–56] Briefly, the interaction forces are obtained by determining the deflection of a force measuring spring supporting the lower surface while the distance between the two surfaces is measured by monitoring the fringes of equal chromatic order (FECO) using a spectrometer. The polymer coated discs were placed in cross cylinder geometry and the measured radius of surface curvature for each contact position was used to normalize the measured force to enable quantitative comparison between different contact positions and experiments. The Derjaguin approximation[57] gives the relationship between the interaction energy per unit area, E, for two flat plates from the measured force–distance, $F(D)$, relationship between two crossed cylinders

$$E(D) = \frac{F(D)}{2\pi R} \qquad (1)$$

The Derjaguin approximation is valid at small distances where $D \ll R$. The radius of curvature was measured for two cross-sections, at 90° and the geometrical mean was used in calculations. For these experiments the measured radius of curvature was 1.0 ± 0.15 cm.

In the present work, normal and shear force profiles between the ATRP grown brushes were measured with a Mark II SFA with a shear device (by SurForce). The shear device includes both a receiver where the top surface was mounted and a bimorph slider device where the lower surface was mounted. As in previous designs,[58,59] application of a triangular signal to the bimorph slider enables linear lateral movement of the lower surface relative to the upper surface, here up to 1 mm.[59] The top receiver assembly has semi-conductor strain gauges to work as a force sensor.

Thickness determination

The thickness in air and the refractive index of the layers was determined by the FECO wavelength positions using a multi-matrix method (MMM)[60] and additional details are provided elsewhere.[48] Briefly, a model of the optical cavity is used to generate the FECO wavelength pattern by MMM with input parameters such as thickness and refractive index of each layer. A fitting algorithm determines the set of parameters that minimizes the difference between the experimental
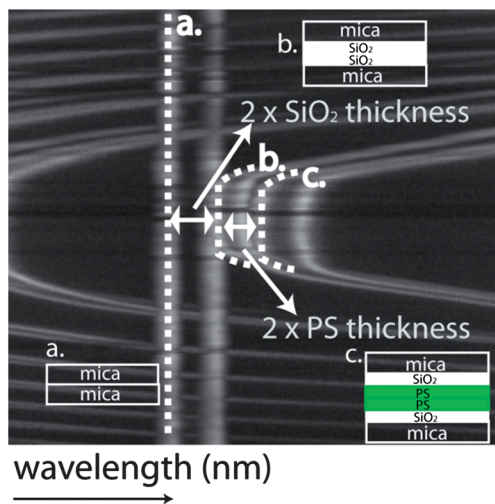
Fig. 1 An example image of how the fringes of equal chromatic order (FECO) wavelengths shift as the number of layers between the surfaces is increased. The optical cavity between the silver layers is modeled and the data fitted to extract the thicknesses and refractive index of the different layers (silver, mica, silica, and polymer) sequentially. The image itself is an overlay of the contact FECO wavelengths for the three measured geometries used; (a) contact of mica–mica surfaces, (b) contact of silica–silica surfaces, (c) contact of PS–PS surfaces. The dashed lines are guides to distinguish different contact geometries.

measurement and the model. Fig. 1 provides an example of the contact fringes obtained from the corresponding geometries of the system where subsequent layers are added to demonstrate how the thickness and refractive index of the various layers (silver, mica, silica, polymer) were determined. First, the bare mica–mica contact (a) was always measured as a control in order to determine the thickness and the refractive index of the silver and mica sheets before adding subsequent layers, e.g. silica and polymer. Next, the contact of silica–silica (b) was measured for identical mica sheets and the thickness and refractive index of the deposited silica film was determined. The accuracy of the fitting program and approach was confirmed by comparing the thickness obtained from ellipsometry to that of multiple experiments with different mica and silica thicknesses. Throughout any given experiment, differences between the control measurements before and after adding additional optical layers were less than 3% in thickness and 1% in refractive index. After establishing the thicknesses and refractive indexes of the silver, mica, and silica layers, the thickness of the ATRP-grown polystyrene was determined be simply fitting the FECO wavelengths of the entire system (c). At least four different positions on the surfaces of different sets of samples were measured to confirm the uniformity of the film.

Normal and shear force measurements of polymer layers

In the normal force setting, after the measurements of the dry PS film thickness, the surfaces were separated a couple of millimeters and the SFA was filled with toluene. The surfaces were brought closer together (≤0.5 mm) and the film was left solvating for 24 hours before measuring the force profile. The distance "D" utilized in the force–distance profiles provided in

the following sections was defined as the spacing between the opposing silica surfaces which corresponds directly to the thickness or extension of the two PS brushes. Multiple compression–decompression cycles for different positions on the surfaces were measured. At least 10 seconds was elapsed after each displacement before taking a reading of the surface separation and 30 minutes was elapsed between different approach/separation cycles to allow for chain relaxation. As is commonly done, the shear force measurements used a droplet of toluene as the shear attachment cannot be fully immersed in solvent.[16] A small vial of toluene was placed inside the SFA chamber during shear measurements to maintain the vapor pressure and minimize evaporation of the toluene droplet between the surfaces. The lateral, parallel movements of the lower surface mounted in the bimorph device were achieved by applying a triangular signal with a function generator (3325B, Hewlett Packard) while a signal conditioning amplifier (2300, Vishey) was used to magnify the signal obtained from the receiver where the upper surface was mounted. The magnified response voltage was collected by a XYt chart recorder (BD41, Kipp&Zonen) and converted to the force (N) between the surfaces. An example of the XYt output is shown in Fig. 2. The applied triangular signal and the detected voltage were monitored simultaneously. The sliding distance and the velocity of the lateral motion from the lower surfaces were controlled by the applied voltage and the frequency of the function generator, respectively. In the present work, the maximum sliding distance was fixed at 1.25 μm while the velocity was 100 nm s^{-1}.

For several measurements, the normal force profile was measured in both the normal and shear force setting to confirm reproducibility, and that the brush layers remained fully solvated in toluene throughout the droplet experiment. The normal force profile and the film thickness were also checked before and after the shear measurements to confirm the stability of the ATRP grown PS brushes. No substantive change in thickness was detected. Both the shear and normal force
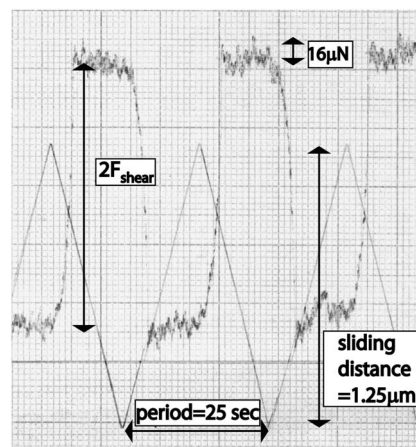

Fig. 2 Example of a XYt plot used for shear force analysis of ATRP grown PS brushes ($D = 1767 \pm 33$ Å). The maximum sliding distance was 1.25 μm obtained from the peak-to-peak value of the triangular wave. The shear force between the opposing PS brushes is denoted as F_{shear} and is determined from the plateau height difference.

Table 1 Characterizations of the ATRP grown polystyrene

Sample	SFA measured			GPC measured		Estimated		
	PS dry thickness (Å)	Measured brush extension h_{exp}, (Å)	mg m^{-2}	MW (kg mol^{-1})	PDI	$\sigma \times 10^2$ (chains per Å^2)	Overlap surface density Σ^a	Fully stretched length L^c, (Å)
A	142 ± 13	630 ± 50	15 ± 1.3	23.5	1.088	0.38	26	588
B	502 ± 36	1950 ± 100	52 ± 3.1	60.5	1.211	0.52	111	1513
C	665 ± 41	2370 ± 125	70 ± 4.5	100.0^d	1.285	0.42	162	2500
D^b	73 ± 13	525 ± 50	7.6 ± 1.0	57.0	1.080	0.08	15.8	1425

^{a} $R_g = 1.86 \times N^{0.595}$ where N = degree of polymerization.[75] ^{b} Physically adsorbed brush formed from a 50 : 50 PS–P2VP diblock copolymer. ^{c} $L = aN$ where a is the repeating PS monomer size of 2.6 Å.[9] ^{d} Estimated based on the inset of Fig. 1 measured by GPC.

measurement were performed in a temperature controlled environment at 25 ± 0.2 °C.

Results and discussions

Brush properties

In this work, the physical properties of ultra-high density PS brushes formed by the "grafting from" method were studied using an SFA. The dimensionless overlap surface density, $\Sigma = \sigma \pi R_g^2$, is typically used to describe and compare different brushes, where σ is the experimental chain grafting density (chains per Å^2), and R_g is the radius of gyration of a free polymer chain in solution.[20] A clear challenge in using "grafting from" brushes is defining the MW and grafting density of the formed polymer brush layer. Fortunately, it is straightforward to measure the dry film thickness and uniformity of the grown film using SFA measurements. Table 1 reports the average measured polymer thickness for three different ATRP grown PS films. The error was established by measuring the film thickness at a minimum of 4 different contact positions between the layers. Given the bulk density of PS, $\rho = 1.05$ g cm^{-3}, the mass per unit area of the grown PS film can be easily calculated from the measured dry thickness. To provide information on the MW of the brush layer, free initiator was present in the reaction solution during our polymerizations. It has been previously reported

that chains grown free in solution provide a good indication of the MW of chains grown simultaneously from initiator layers from the surface.[50,61–63] The MW and PDI of the free chains in the polymerization supernatant were determined by GPC. These values *versus* the measured dry film thickness are reported in Table 1 and plotted in the inset of Fig. 3. Typically, a linear increase in dry film thickness with MW is expected and has been reported in earlier studies. In this work, the two lower MW ($\Sigma = 26$ and 111) polymerizations follow a linear increase in film thickness. However, the thickest film, which also had the highest PDI, clearly deviates significantly from this trend. This deviation between the surface and supernatant chains at high polymerizations is attributed to chain termination events in the surface film for thicker, high MW polymers. Even with this caveat, the supernatant measurements of MW and PDI do provide an estimate of the surface grown polymer film properties and three clearly different conditions were achieved (Table 1). The calculated value of $\Sigma \sim 191$ for the thickest film is likely a significant overestimation. Based on the measured film thickness, a more modest MW of ~100k yields an $\Sigma \sim 162$.

Force profile measurements

The interaction force profiles as a function of distance for three different ATRP grown PS films in toluene are now described. As will be discussed in the next section, significant hysteresis was observed in the normal force measurements. The data reported in Fig. 3 were measured after allowing the systems to relax for at least 24 hours before compressing. The extension of the brush in toluene, as depicted by the arrows in Fig. 3, was defined as the onset of the repulsive force under these equilibrated conditions (Table 1). The onset distance increases with the thickness of the dry PS film, consistent with the expected increase in the grafted brush MW with increasing film thickness. With further compression, the repulsive force increased monotonically with decreasing separation. One fact that needs to be noted here is that unlike the grafting-to brushes, the extensions of the ATRP grown PS were very close to or even exceeded the fully stretched length based on the GPC measurements. Although the PDI of the chains can account for this discrepancy, the GPC results from the supernatant chains should only be considered a rough indication of the MW and PDI of the surface grafted chains. The primary characterization
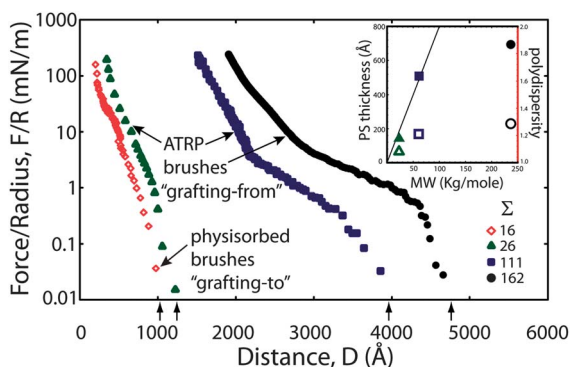

Fig. 3 Measured force profiles of ATRP grown PS brushes for three different grafting densities (solid symbols). Force profile data for a well-defined brush formed from a 50 : 50 PS–P2VP diblock copolymer with $\Sigma = 16$ (diamonds) is also shown for comparison. The inset shows the relationships among dry PS thickness (closed symbols), MW and the polydispersity (opened symbols) determined by GPC.

of the surface films is obtained by direct measurement of the film thickness and solvated brush extension by SFA.

For comparison, the force to compress a physically adsorbed brush formed from a 50 : 50 polystyrene-*b*-poly-(2-vinylpyridine) (PS–P2VP) diblock copolymer with $\Sigma = 16$ is also shown. The physical properties of this well-defined "grafted to" brush are also provided in Table 1. As can be seen, the force profile for this PS–P2VP brush (PS MW = 57k) is very similar to that of the $\Sigma \sim 26$ ATRP PS brush (MW$_{estimate}$ = 23.5k). Moreover, both the ∼PDI and dry film thickness are very similar for both of these cases although their MWs may differ by almost a factor of 3. In contrast, the high MW ATRP brushes ($\Sigma \sim 111, 162$) have a more diffuse outer brush region, thus, a soft long-range repulsion due to their greater polydispersity and MW. The softer repulsion further suggests that the GPC measurements should be considered as a lower bound estimate for the grafted brush PDI. Although the MW of the PS diblock matches the $\Sigma \sim 111$ ATRP PS brush (MW$_{estimate}$ = 60.5k), the brush extension is much longer with the ATRP brush due to the presumably large increase in grafting density. To the best of our knowledge, these are the highest grafting density brushes for which interaction force profiles have been measured.

The measured repulsive force was also compared to the self-consistent mean field theory developed by Milner, Witten and Cates (MWC) for two polymer brushes in good solvent conditions[18,38,64]

$$F(D)/R = 2\pi h_0 \sigma^{4/3} \nu^{2/3} \omega^{1/3}(1/u + u^2 - u^5/5 - 9/5)$$

where $u = h/h_0$, h_0 is defined as the unperturbed extension of the monodisperse brush calculated from $h_0 = (12/\pi^2)^{1/3} N \sigma^{1/3} \omega^{1/3} \nu^{-1/3}$, ω is the excluded volume parameter, and the effective size parameter ν, which has the dimension of length^{-2}, is found from the statistical segment size, b, using $\nu = 3/b^2$. The values of ω and b used were $(3.2 \text{ Å})^3$ and 7.6 Å, respectively, based on the work with a similar ATRP system carried out by Ell *et al.*[50] As

shown in Fig. 4 for $\Sigma \sim 26$ the MWC prediction matches reasonably well to the measured force after repeated compression and separation cycles. As originally demonstrated by Milner and subsequently others,[37,65,66] a small increase in the chain PDI leads to a significant increase in the onset of the measured repulsion between opposing polymer brushes as observed here. It is, however, somewhat surprising that the MWC theory provides a reasonable estimate given that the theory assumes dilute/semi-dilute polymer concentration and simple pairwise interactions. The strong stretching limit is likely more reasonable for these high grafting density brushes than more typical, lower density "grafting-to" brushes.[65] Based on our estimated grafting density of $\Sigma \sim 26$, the average concentration within the polymer brush was already significantly above the limit of the semi-dilute concentration range.[67] Not surprisingly, at the higher grafting densities, $\Sigma \sim 111$ and 162, the agreement was very poor. However, the MW and polydispersity of the grafted brushes may not be well represented by the measured values for free chains in solution during the polymerization. For thicker films, it is more difficult to maintain a constant growth rate and there is a greater chance for chain transfer termination events between neighboring chains.[68]

A more interesting feature of the grafted brushes is the significant hysteresis observed in the force profiles, where the measured interaction force upon separation was much less than that on surface approach. Such behavior has only rarely been reported between end-grafted polymer brushes in good solvent conditions. Indeed, the only examples we are aware of also studied polydisperse, "grafting-from" polymer brushes[37,45,69] and "grafting-to" system with high MW and polydispersity.[28,69] More commonly, hysteresis is observed under poor solvent conditions where the polymer layers are somewhat adhesive; there is incomplete brush coverage on the surfaces resulting in bridging interactions; or, the polymer film is adsorbed and undergoes long-lived structural rearrangements during the measurements. Examples of compression–decompression cycles of our ATRP brushes are shown in Fig. 4 for $\Sigma \sim 26$ and $\Sigma \sim 111$. The solid and empty symbols represent the compression and decompression processes, respectively, while the solid and dashed lines with arrow heads are provided as a guide to distinguish different approach and separation cycles. The initial compression was carried out on equilibrated brushes that had been allowed to relax for at least 24 hours before compressing. After each surface displacement during the force measurement, the brushes were allowed to relax for 8–12 seconds before measuring the surface separation. The average approach rate is reported in Fig. 4. Similar behavior is observed for the three ATRP brush systems where the brush extension becomes less for subsequent compression–decompression cycles. The magnitude of the hysteresis increases with the polydispersity and thickness (MW) of the brush layer. With increased cycling, the curves collapse to a master interaction force profile that is similar to that expected for a more mono-disperse brush system. In other words, with cycling the force is dominated by the osmotic repulsion rather than the details of the brush structure. These findings suggest that the structure of the diffuse outer layer of the brush is greatly modified by
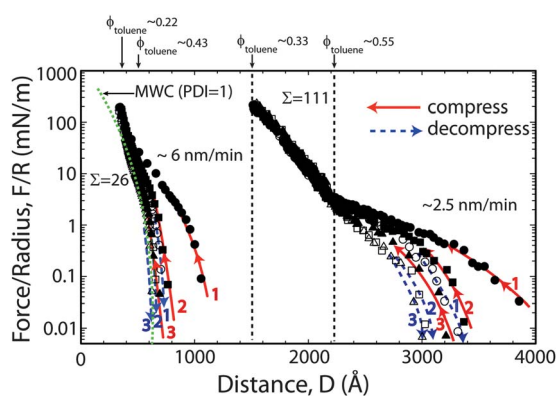

Fig. 4 Compression–decompression cycles for forces profiles of two opposing ATRP grown PS brushes in toluene with overlap surface density $\Sigma = 26$ and 111. Solid symbols and empty symbols with corresponding shapes represent a single compression and decompression cycle, respectively. The solid and dashed lines with arrowheads are the guides to the eye. At least 30 minutes between different cycles and 8–12 seconds between each surface displacement were allowed for brush relaxation. The average approach rates for each system are provided. The long-dashed line shows the predictions of mono-disperse MWC theory for $\Sigma = 26$.

compression and takes a significant time to relax back to a more equilibrium state. Osaki *et al.*[70] developed an empirical formula to calculate the relaxation time of a polymer in semi-dilute solution by modeling the dynamic modulus using the Rouse model. Using this method, the relaxation time over our polymer MW range is on the order of 10^{-2} seconds – much faster than the experimental time scale of the force profile measurements. Indeed, the experimental time scale is minimally three orders of magnitude longer, but still not sufficient for the system to equilibrate. The entanglement MW of PS in melt is $\sim$18 kg mol^{-1},[71] and increases with decreasing polymer volume fraction with a $-4/3$ power.[46,72] All the studied ATRP brushes are above the entanglement MW and the much higher relaxation time and highly hysteric behavior observed with ATRP-formed brushes increases with MW consistent with a contribution from entanglements effects. In contrast, most physisorbed brushes formed by grafting-to method are below the entanglement MW once the polymer volume fraction is accounted for. Scaling the Rouse time by a factor of $N^{1 \text{ or } 1.4}$ to estimate the reptation time would increase the relaxation time for the lower MW $\sim$ 23.5k by at least two to three orders of magnitude with an additional order of magnitude for the highest MW $\sim$ 100k. Thus, chain entanglements likely contribute to the highly hysteric behavior observed with the ATRP brushes. Even longer relaxation times would be obtained using an arm retraction model.

Shear force measurements

Lateral shear force measurements were carried out on the thickest ATRP brush layer, $\Sigma \sim 162$. In particular, we were very interested in determining the friction behavior as this brush system had the highest hysteresis in the compression cycles. Fig. 5 plots both the normal and shear force as a function of separation between the brush layers. Again, the high hysteresis in the normal force profiles demonstrate that the experimental time scale is shorter than the relaxation process of the brush layer. Surprisingly, lateral shear force was undetectable within the experimental resolution until the opposing layers were

Fig. 5 Normal and shear forces as a function of separation between two opposing ATRP grown PS brushes with $\Sigma = 162$ in toluene. Four compression (closed symbols)–decompression (open symbols) cycles are shown. The solid and dashed lines are the guides to the eye for the different compression–decompression cycles. Shear force measurements (2nd Y axis) were carried out with a velocity of 0.1 μm s^{-1} and sliding distance of 1.25 μm.

highly compressed. This demonstrates that these polydisperse brushes provide an excellent lubrication layer. Even at a volume fraction of only 34% toluene the effective friction coefficient of the layers was less than 0.02. It is commonly suggested that the friction force between polymer brush layers originates from viscous dissipation within the mutual interpenetration region of the opposing polymer brushes.[29,30] Based on MD simulations, Spirin *et al.*[73] have suggested that two types of entanglements need to be taken into consideration in polymer brush systems during sliding; intra-brush entanglements inside an individual brush layer and inter-brush entanglements that occur between the opposing brush layers. As no adhesion was observed between the brush layers during force compression measurements, the findings suggest that intra-brush entanglements within each brush layer increase during compression. These intra-brush entanglements are more dominate than inter-brush entanglements between the two brushes which reduces opposing brush interpenetration and enables low friction sliding between the brushes even under high compression. The importance of intra-brush entanglement behavior is also consistent with the hysteresis observed by Ruths *et al.*[37] with ultra high polydisperse ATRP brushes.

The low friction sliding of these ultra-high density brushes is even more remarkable given the low solvation of the brushes. By using flat contact of two opposing brush layers in air, the baseline ($\Phi_{toluene} = 0$) is well defined and the separation distance under solvated conditions can be directly converted to the volume fraction of polymer and solvent. The friction force between the brushes only becomes measurable when the volume fraction of toluene drops below 34%. After this point, the friction rapidly increases as the brushes are further compressed. Kobayashi *et al.*[42] also observed better lubricant performance for high density P(MPC) brushes in reduced solvent conditions. In this case, the friction was significantly lower in a high-humidity environment compared to that when fully hydrated in water. Similar to the argument presented here, Kobayashi *et al.* suggested that inter-brush contacts and greater interpenetration occurred in bulk water (better solvent quality) compared to high humidity conditions (less good solvent quality).

An important consideration for understanding the properties of high density brushes is possible changes in solvent quality with compression. All the brush systems reported here greatly exceed the semi-dilute regime. Thus, as the brushes are compressed and the polymer concentration in the gap between the surfaces increases, the solvent quality can be significantly reduced resulting in more favorable polymer contacts.[74] This is consistent with more intra- and inter-brush contacts. In addition, the reduction in the solvent quality will substantially decrease the extension of the polymer brushes, which may also reduce the interpenetration region.[31,32] For higher grafting densities ($\Sigma = 111$ and 162), the observed force profiles can be reasonably divided into two distinct concentration ranges: a highly hysteretic region and a reversible region after multiple compressions. These regions correspond to less dense outer brush layer and more dense or collapsed inner brush layer, respectively. The denser region could be possibly attributed to the entanglement network formed during the process of
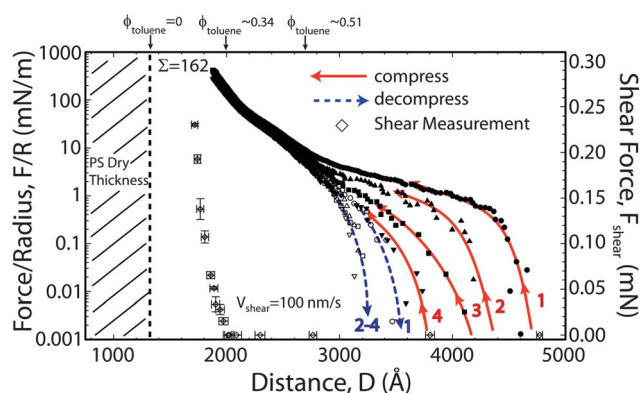
chain-transfer termination when the polymerization was conducted at higher temperature[68] while other "escaped" chains continue growing linearly and created a less dense outer region. Without sufficient relaxation time, the extension of the brush from the dense region is greatly diminished presumably due to formation of favorable intra-brush contacts under solvent starved conditions and the greater entanglements in the system compared to lower density grafted to systems. Likewise, interbrush contacts become more favorable and with high compression ($\Phi < 35\%$) the friction increases rapidly. For lower compressions the outer region of the brush layers remain well solvated and provide frictional properties similar to semi-dilute brushes that have been commonly studied in the past.

Conclusion

Both normal and shear interactions between ultra-high grafted polymer brushes have been examined in the present work. Very long relaxation times are evident from the observed hysteresis with compression–separation cycles. The hysteresis increases with increasing brush MW and polydispersity. Remarkably, the friction behavior is found to be very similar to low density brushes in the semi-dilute regime and does not increase appreciably until the solvent volume fraction is less than 35%. The importance of the high density brushes yielding favorable lubrication properties is that a highly durable lubricating layer can be formed. These findings demonstrate that high grafting density brushes with high polydispersity – a real system rather than ideal monodisperse system – have potential as lubricants in more practical applications.

References

1 J. Klein, Y. Kamiyama, H. Yoshizawa, J. N. Israelachvili, G. H. Fredrickson, P. Pincus and L. J. Fetters, *Macromolecules*, 1993, **26**, 5552–5560.

2 F. Brochard-Wyart, P. G. de Gennes, L. Leger, Y. Marciano and E. Raphael, *J. Phys. Chem.*, 1994, **98**, 9405–9410.

3 C. Devaux, J. P. Chapel, E. Beyou and P. Chaumont, *Eur. Phys. J. E: Soft Matter Biol. Phys.*, 2002, **7**, 345–352.

4 S. T. Milner, *Science*, 1991, **251**, 905–914.

5 P. G. de Gennes, *Macromolecules*, 1980, **13**, 1069–1075.

6 B. Zhao and W. J. Brittain, *Prog. Polym. Sci.*, 2000, **25**, 677–710.

7 M. S. Kent, L. T. Lee, B. J. Factor, F. Rondelez and G. S. Smith, *J. Chem. Phys.*, 1995, **103**, 2320–2342.

8 F. Goujon, P. Malfreyt and D. J. Tildesley, *Mol. Phys.*, 2005, **103**, 2675–2685.

9 C. Devaux, F. Cousin, E. Beyou and J. P. Chapel, *Macromolecules*, 2005, **38**, 4296–4300.

10 S. Alexander, *J. Phys.*, 1977, **38**, 983–987.

11 S. Alexander, *J. Phys.*, 1977, **38**, 977–982.

12 P. G. De Gennes, *Macromolecules*, 1981, **14**, 1637–1644.

13 S. T. Milner, T. A. Witten and M. E. Cates, *Europhys. Lett.*, 1988, **5**, 413–418.

14 S. T. Milner, T. A. Witten and M. E. Cates, *Macromolecules*, 1988, **21**, 2610–2619.

15 H. J. Taunton, C. Toprakcioglu, L. J. Fetters and J. Klein, *Macromolecules*, 1990, **23**, 571–580.

16 S. M. Kilbey, F. S. Bates, M. Tirrell, H. Yoshizawa, R. Hill and J. Israelachvili, *Macromolecules*, 1995, **28**, 5626–5631.

17 S. M. Kilbey, H. Watanabe and M. Tirrell, *Macromolecules*, 2001, **34**, 5249–5259.

18 J. Alonzo, J. W. Mays and S. M. Kilbey II, *Soft Matter*, 2009, **5**, 1897–1904.

19 M. S. Kent, L. T. Lee, B. Farnoux and F. Rondelez, *Macromolecules*, 1992, **25**, 6240–6247.

20 R. Baranowski and M. D. Whitmore, *J. Chem. Phys.*, 1998, **108**, 9885–9892.

21 R. Baranowski and M. D. Whitmore, *J. Chem. Phys.*, 1995, **103**, 2343–2353.

22 G. S. Grest, *J. Chem. Phys.*, 1996, **105**, 5532–5541.

23 G. S. Grest, *Macromolecules*, 1994, **27**, 418–426.

24 C. Pastorino, K. Blinder, T. Kreer and M. Muller, *J. Chem. Phys.*, 2006, **124**, 064902.

25 I. G. Elliott, T. L. Kuhl and R. Faller, *Macromolecules*, 2010, **43**, 9131–9138.

26 J. Klein, E. Kumacheva, D. Mahalu, D. Perahia and L. J. Fetters, *Nature*, 1994, **370**, 634–636.

27 J. Klein, D. Perahia and S. Warburg, *Nature*, 1991, **352**, 143–145.

28 U. Raviv, R. Tadmor and J. Klein, *J. Phys. Chem. B*, 2001, **105**, 8125–8134.

29 J. Klein, E. Kumacheva, D. Perahia and L. J. Fetters, *Acta Polym.*, 1998, **49**, 617–625.

30 R. Tadmor, J. Janik, J. Klein and L. J. Fetters, *Phys. Rev. Lett.*, 2003, **91**, 115503.

31 P. A. Schorr, T. C. B. Kwan, S. M. Kilbey, E. S. G. Shaqfeh and M. Tirrell, *Macromolecules*, 2003, **36**, 389–398.

32 A. M. Forster, J. W. Mays and S. M. Kilbey, *J. Polym. Sci., Part B: Polym. Phys.*, 2006, **44**, 649–655.

33 G. S. Grest, *Phys. Rev. Lett.*, 1996, **76**, 4979–4982.

34 T. A. Witten, L. Leibler and P. A. Pincus, *Macromolecules*, 1990, **23**, 824–829.

35 T. Kreer, M. H. Muser, K. Binder and J. Klein, *Langmuir*, 2001, **17**, 7804–7813.

36 M. Ejaz, S. Yamamoto, K. Ohno, Y. Tsujii and T. Fukuda, *Macromolecules*, 1998, **31**, 5934–5936.

37 M. Ruths, D. Johannsmann, J. Ruhe and W. Knoll, *Macromolecules*, 2000, **33**, 3860–3870.

38 S. T. Milner, T. A. Witten and M. E. Cates, *Macromolecules*, 1989, **22**, 853–861.

39 S. Yamamoto, M. Ejaz, Y. Tsujii, M. Matsumoto and T. Fukuda, *Macromolecules*, 2000, **33**, 5602–5607.

40 S. Yamamoto, M. Ejaz, Y. Tsujii and T. Fukuda, *Macromolecules*, 2000, **33**, 5608–5612.

41 P. G. de Gennes, *Adv. Colloid Interface Sci.*, 1987, **27**, 189–209.

42 M. Kobayashi, Y. Terayama, N. Hosaka, M. Kaido, A. Suzuki, N. Yamada, N. Torikai, K. Ishihara and A. Takahara, *Soft Matter*, 2007, **3**, 740–746.

43 Y. Sakata, M. Kobayashi, H. Otsuka and A. Takahara, *Polym. J.*, 2005, **37**, 767–775.

44 M. Kobayashi and A. Takahara, *Chem. Lett.*, 2005, **34**, 1582.

45 I. E. Dunlop, W. H. Briscoe, S. Titmuss, R. M. J. Jacobs, V. L. Osborne, S. Edmondson, W. T. S. Huck and J. Klein, *J. Phys. Chem. B*, 2009, **113**, 3947–3956.

46 R. H. Colby, M. Rubinstein and J. L. Viovy, *Macromolecules*, 1992, **25**, 996–998.

47 G. Vigil, Z. Xu, S. Steinberg and J. Israelachvili, *J. Colloid Interface Sci.*, 1994, **165**, 367–385.

48 R. Orozco-Alcaraz and T. L. Kuhl, *Langmuir*, 2013, **29**, 337–343.

49 K. Matyjaszewski, P. J. Miller, N. Shukla, B. Immaraporn, A. Gelman, B. B. Luokala, T. M. Siclovan, G. Kickelbick, T. Vallant, H. Hoffmann and T. Pakula, *Macromolecules*, 1999, **32**, 8716–8724.

50 J. R. Ell, D. E. Mulder, R. Faller, T. E. Patten and T. L. Kuhl, *Macromolecules*, 2009, **42**, 9523–9527.

51 J. Xia and K. Matyjaszewski, *Macromolecules*, 1997, **30**, 7697–7700.

52 J. N. Israelachvili, *J. Colloid Interface Sci.*, 1973, **44**, 259–272.

53 J. N. Israelachvili and G. E. Adams, *Nature*, 1976, **262**, 774–776.

54 J. N. Israelachvili and G. E. Adams, *J. Chem. Soc., Faraday Trans. 1*, 1978, 975–1001.

55 J. N. Israelachvili and M. McGuiggan, *J. Mater. Res.*, 1990, **5**, 2223–2231.

56 J. L. Parker, H. K. Christenson and B. W. Ninham, *Rev. Sci. Instrum.*, 1989, **60**, 3135–3138.

57 B. V. Derjaguin, *Kolloid-Z.*, 1934, **69**, 155–164.

58 J. Israelachvili, *Proc. Natl. Acad. Sci. U. S. A.*, 1987, **84**, 4722–4724.

59 G. Luengo, F. J. Schmitt, R. Hill and J. Israelachvili, *Macromolecules*, 1997, **30**, 2482–2494.

60 M. T. Clarkson, *J. Phys. D: Appl. Phys.*, 1989, **22**, 475.

61 M. Biesalski and J. Rühe, *Macromolecules*, 2001, **35**, 499–507.

62 M. Biesalski and J. Rühe, *Macromolecules*, 1999, **32**, 2309–2316.

63 T. Wu, P. Gong, I. Szleifer, P. Vlček, V. Šubr and J. Genzer, *Macromolecules*, 2007, **40**, 8756–8764.

64 S. T. Milner, *Europhys. Lett.*, 1988, **7**, 695–699.

65 J. U. Kim and M. W. Matsen, *Macromolecules*, 2009, **42**, 3430–3432.

66 W.-P. Liao and T. L. Kuhl, *Macromolecules*, 2012, **45**, 5766–5772.

67 I. Noda, Y. Higo, N. Ueno and T. Fujimoto, *Macromolecules*, 1984, **17**, 1055–1059.

68 A. Samadi, S. M. Husson, Y. Liu, I. Luzinov and S. Michael Kilbey, *Macromol. Rapid Commun.*, 2005, **26**, 1829–1834.

69 J. N. Israelachvili, R. K. Tandon and L. R. White, *J. Colloid Interface Sci.*, 1980, **78**, 430–443.

70 K. Osaki, T. Inoue, T. Uematsu and Y. Yamashita, *J. Polym. Sci., Part B: Polym. Phys.*, 2001, **39**, 1704–1712.

71 S. Onogi, T. Masuda and K. Kitagawa, *Macromolecules*, 1970, **3**, 109–116.

72 H. Tao, C.-i. Huang and T. P. Lodge, *Macromolecules*, 1999, **32**, 1212–1217.

73 L. Spirin, A. Galuschko, T. Kreer, A. Johner, J. Baschnagel and K. Binder, *Eur. Phys. J. E: Soft Matter Biol. Phys.*, 2010, **33**, 307–311.

74 Z. W. Zhou and P. J. Daivis, *J. Chem. Phys.*, 2009, **130**, 224904–224910.

75 Y. Higo, N. Ueno and I. Noda, *Polym. J.*, 1983, **15**, 367–375.